JURNAL ILMIAH MEDICAMENTO

Vol.12 No.1 (March 2026)
page 131-145
https://doi.org/10.36733/medicamento.v12i1.12687
e-ISSN: 2356-4814

Original Article

Revealing Phytopharmaceutical Insights into Jaras Gambo Extract from *Uncaria gambir* Roxb. against Breast Cancer Using Network Pharmacology and ADME/Tox Approach

Rafiqah Nur Viviani[1,2], Nathasya Shasykirana Mahendra[1,2], Shaum Shiyan[1,2*], Galih Pratiwi[3]

[1]Department of Pharmacy, Faculty of Mathematics and Natural Sciences, Universitas Sriwijaya, Indralaya, Indonesia
[2]Phytopharmaceutic Research Center (PRC), Department of Pharmacy, Universitas Sriwijaya, Indralaya, Indonesia
[3]Department of Pharmacy, Faculty of Health and Technology, Universitas Aisyiyah Palembang, Palembang, Indonesia

Submitted : 07-10-2025
Revised : 11-03-2026
Accepted : 21-03-2026

Keywords: breast cancer, gambo, molecular docking, network pharmacology, phytopharmaceutical, *Uncaria gambir* Roxb.

Correspondence:
Shaum Shiyan
shaumshiyan@unsri.ac.id

Abstract

Background: Breast cancer remains a leading cause of mortality in women and demands multi-target strategies that can address pathway redundancy and resistance.

Objective: This study aimed to characterize the bioactive constituents of Jaras Gambo Toman extract and evaluate its potential anti-breast cancer activity through an integrated network pharmacology and molecular docking approach.

Methods: Jaras Gambo (processed gambier sap mass; *Uncaria gambir* Roxb.) collected in Babat Toman, South Sumatra, was macerated in ethanol, and the macerate was then filtered and concentrated to obtain a crude extract. Its constituents were profiled by liquid chromatography–high-resolution mass spectrometry (LC–HRMS). Network pharmacology (target prediction, pathway enrichment, and drug-likeness/toxicity screening) was integrated with structure-based molecular docking to prioritize active constituents and predict their interactions with breast cancer–related proteins.

Results: The results of the analysis show therapeutic potential through the significant binding affinity between the bioactive components of the extract and proteins in the regulation of cancer cell proliferation and apoptosis, particularly AKT1, TP53, BCL2, TNF, and EGFR. Molecular interactions are suggested by favorable *binding affinity* parameters accompanied by the formation of hydrogen and hydrophobic bonds at the active sites of key residues. The involvement of several signaling pathways, such as the PI3K/AKT pathway, p53 signaling pathway, and TNF signaling pathway, may represent key mechanistic pathways of bioactive compounds in targeting disease proteins. Further characterization showed that there are eight main active components, including chlorogenic acid, isoquercitrin, morin hydrate, naringenin, quercetin, eriodictyol, ribofuranoside, and scopoletin, which showed docking profiles comparable to erlotinib across selected targets.

Conclusion: These results suggest the potential of Jaras Gambo Toman extract as a potential source of multi-target bioactive compounds for further breast cancer research.

How to Cite: (*citation style* AMA 11th Ed.)
Viviani RN, Mahendra NS, Shiyan S, Pratiwi G. Revealing Phytopharmaceutical Insights into Jaras Gambo Extract from *Uncaria gambir* Roxb. against Breast Cancer Using Network Pharmacology and ADME/Tox Approach. *J. Ilm. Medicam.*, 2026;12(1): 131-145. https://doi.org/10.36733/medicamento.v12i1.12687

INTRODUCTION

Breast cancer remains the most commonly diagnosed malignancy in women and a leading cause of cancer mortality, with outcomes constrained by molecular heterogeneity, primary and acquired resistance, and cumulative toxicities of long-term therapy[1–3]. Although subtype-directed regimens (endocrine therapy, human epidermal growth factor receptor 2 (HER2) blockade, cyclin-dependent kinase 4 and 6 (CDK4/6) and phosphoinositide 3-kinase (PI3K) inhibitors) have extended survival, many patients still experience relapse or intolerance, underscoring the need for complementary strategies that modulate multiple signaling axes simultaneously[4,5]. In this context, rational exploration of phytochemical mixtures has re-emerged, not as folklore validation, but as a systems-level approach to engage convergent nodes across proliferation, survival, inflammation, and stress responses[6,7].

In South Sumatra, *Uncaria gambir* Roxb. is locally known as Gambo and traditionally processed into jaras, a solid processed sap mass produced through conventional gambier preparation. For this study, jaras was collected

specifically from Babat Toman, Musi Banyuasin (South Sumatra, Indonesia)—a long-standing production area of socioeconomic importance. Hereafter, this material is referred to as Jaras Gambo Toman (JGT). Chemically, Gambo-derived materials are rich in catechin-type phenolics and related flavonoids that have been linked to redox modulation, anti-inflammatory activity, and growth control in diverse biological systems—properties mechanistically relevant to breast cancer biology[8]. Consistent with this premise, catechin shows cytotoxicity with an IC_{50} of 22.91 µg/mL, and recent nanoformulation studies of catechin-rich gambir demonstrate strengthened anticancer signals in breast models—markedly enhanced cytotoxicity against T47D cells compared with crude extract, together with chemopreventive effects in a benzo[a]pyrene mouse model that preserve antioxidant defenses and suppress TNF-α[9,10]. Yet, a coherent map connecting jaras from Babat Toman to breast cancer-relevant targets and pathways has not been established.

Network pharmacology provides a tractable framework to deconvolute such multi-component matrices by projecting curated phytochemicals onto disease gene sets and protein–protein interaction (PPI) graphs, thereby revealing hub proteins and enriched pathways most likely to govern phenotype-level responses[11–13]. When paired with in silico ADME/Tox triage, this strategy prioritizes constituents with plausible oral exposure and manageable safety liabilities, reducing the risk of chasing purely structural false positives[14]. Structure-based molecular docking offers orthogonal evidence by testing whether top-ranked ligands can plausibly engage functionally relevant binding pockets in targets highlighted by the network[15,16].

Here, we integrated these complementary approaches to investigate Jaras Gambo Toman (JGT). We first assembled and standardized the phytochemical space of the JGT material, then combined ligand-based target prediction with disease-gene mapping to delineate a candidate target set for breast cancer. We next constructed PPI networks and performed functional enrichment to identify signaling axes consistently engaged by JGT constituents, with emphasis on canonical hallmarks such as PI3K/AKT, MAPK, apoptosis, and cell-cycle control. To refine tractability, we applied ADME/Tox filters and finally performed molecular docking against selected hub proteins to probe structural plausibility.

We aim (i) to construct a comprehensive network view relating JGT to breast cancer-relevant targets and pathways, and (ii) to extract a small, experimentally tractable panel of compound–target–pathway candidates. By coupling regional provenance with mechanistic resolution, this work elevates a South Sumatra resource from local utility to translational hypotheses with clear next steps in oncology research.

METHODS

This was an in silico, ligand-centric pharmacology study anchored to a locally sourced botanical input (JGT extract), integrating LC–HRMS profiling, activity/target prediction, network pharmacology, ADME/Tox triage, and molecular docking.

Tools and Materials

Tools. The specialized equipment comprised an Orbitrap LC–HRMS system (Q Exactive™ Plus, Thermo Fisher Scientific, Bremen, Germany), an analytical balance (OHAUS Adventurer, 0.1 mg readability, USA), a laboratory oven (Memmert, Schwabach, Germany), a magnetic stirrer/hotplate (IKA C-MAG HS 4, Staufen, Germany), a rotary evaporator (RE-2010VN), a vortex mixer (Scilogex MX-S, USA), and an ultrasonic bath (Redsun unit). In silico analyses were performed on an Apple MacBook Air M1 (8-GB RAM, 512-GB SSD) and a Lenovo ThinkPad X270 (8-GB RAM, 512-GB SSD). Software and versions: Cytoscape v3.10.x, STRING, STITCH, PASS Online, SwissTargetPrediction, SwissADME, MolSoft, OpenBabel 2.4.1, MGLTools 1.5.7, AutoDock Vina 1.2.3, PyMOL, BIOVIA DS Visualizer.

Materials. The plant-derived material was JGT extract—the ethanolic extract of jaras, a processed sap mass obtained from *Uncaria gambir* Roxb. (locally, Gambo) collected in Babat Toman, Musi Banyuasin, South Sumatra, Indonesia. Extraction employed analytical-grade 96% ethanol and purified water (aquadest), both sourced from Djiwa Labor, Indonesia. For docking benchmarks, the reference ligand erlotinib was obtained as a 3D structure from PubChem. Public databases included the Protein Data Bank (PDB) for experimentally solved protein structures and GeneCards for disease-gene sets; tentative metabolite identifications from LC–HRMS were supported by searches against established spectral/compound libraries.

Research Procedure

Preparation of JGT Extract

Jaras was milled to a fine powder and macerated with 96% ethanol at room temperature for 24 h with intermittent stirring. The mixture was clarified by decantation, and the supernatant was concentrated under reduced

pressure using rotary evaporator to yield JGT extract, which was stored at 4 °C in amber glass until analysis and re-dissolved in LC-grade solvent immediately before LC–HRMS[17].

LC–HRMS Profiling of JGT Extract

Aliquots of the JGT extract were injected into the Q Exactive Plus under routine small-molecule conditions (positive/negative ESI as appropriate). Accurate-mass features were processed to assign tentative compounds and identities by matching to public spectral/compound libraries and primary literature on *U. gambir*[18]. LC–HRMS profiling was performed to prioritize the major constituents of the JGT extract. The observed LC–HRMS parameters used in this study included the annotated compound identity, predicted molecular formula, maximum peak area, and semi-quantitative yield (%). These parameters were used to rank the detected constituents according to their relative abundance. The annotated compounds were then consolidated into a non-redundant list, and their chemical structures were standardized into canonical Simplified Molecular Input Line Entry System (SMILES) strings for subsequent cheminformatics and network pharmacology analyses.

Ligand-based Activity Prediction

Curated compounds from the LC–HRMS list (**Table 1**) were standardized to canonical SMILES and submitted to PASS Online (https://www.way2drug.com/passonline/predict.php) to obtain probabilities of activity (Pa) for oncology-relevant terms, such as antineoplastic breast cancer, apoptosis, and chemopreventive. In line with common PASS usage, $Pa \geq 0.70$ was considered strong a priori evidence of activity, while $0.50 < Pa < 0.70$ indicated moderate likelihood[19].

Target Prediction and Disease-gene Mapping

For each compound, putative human protein targets were predicted using SwissTargetPrediction (https://www.swisstargetprediction.ch/; organism: Homo sapiens. Breast cancer-associated genes were retrieved from GeneCards (https://www.genecards.org/) by querying “breast cancer” and applying a relevance-score threshold. The intersection between predicted targets and disease genes defined the candidate target set for subsequent network analysis. Where helpful to illustrate set overlap, Venn diagrams were generated with the PSB Ugent web tool (https://bioinformatics.psb.ugent.be/webtools/Venn/)[20].

PPI Network Construction and Pathway Enrichment

Predicted human targets of the JGT extract were intersected with a breast cancer gene set and the resulting candidates were submitted to STRING (https://string-db.org/; organism: Homo sapiens) to assemble a protein-protein interaction (PPI) graph. We used the evidence-integrated interaction score with a minimum required score of 0.40, enabling literature, experimental, co-expression, and database channels; disconnected singletons were retained for transparency but excluded from centrality statistics. The STRING-exported network was imported into Cytoscape v3.10.x. We report degree, betweenness, and closeness centralities to flag hubs and bottlenecks a priori, and annotate high-confidence edges in the figures. Where compound–protein relationships aided interpretation, STITCH overlays (https://stitch.embl.de/) were harmonized onto the PPI layer to render compound–target–pathway views[20,21].

Functional over-representation was performed in STRING on the same candidate set against three curated libraries—Gene Ontology: Biological Process (GO BP), KEGG signaling pathways, and Reactome pathways—using STRING’s hypergeometric framework with Benjamini–Hochberg false-discovery rate (FDR) correction. Unless otherwise specified, significance was defined as FDR-adjusted $p < 0.05$, and we report each term’s gene ratio (hits/query size), leading-edge genes, and FDR.

Drug-likeness, ADME, and In silico Toxicity Triage

Drug-likeness was evaluated exclusively under Lipinski’s Rule of Five using SwissADME (https://www.swissadme.ch/) and Molsoft (https://molsoft.com/mprop/)[22]. For each JGT extract constituent, we recorded molecular weight (MW), calculated lipophilicity (cLogP), hydrogen-bond donors (HBD), and hydrogen-bond acceptors (HBA). Compounds passing Ro5 were defined as those meeting all four thresholds—$MW \leq 500$ g·mol^{-1}, $cLogP \leq 5$, $HBD \leq 5$, and $HBA \leq 10$. Prospective safety risks were screened with Deep-PK (https://biosig.lab.uq.edu.au/deeppk/prediction).

Molecular Docking and Pose Validation

Hub proteins prioritized from the network analysis—AKT1 (PDB 2UVM), TNF (6OOY), EGFR (4JQ7), TP53 (1XQH), and BCL2 (2W3L)—were prepared from RCSB PDB entries by retaining relevant chains/cofactors, removing non-essential crystallographic waters, adding polar hydrogens, and assigning Gasteiger charges (MGLTools 1.5.7) at approximate physiological pH. Small molecules from the JGT extract were retrieved as 3D structures from PubChem[20]. Redocking of the native co-crystal ligand into its cognate receptor was used to verify the search space and scoring; solutions with RMSD ≤ 2.0 Å relative to the crystallographic pose (measured in PyMOL) were deemed acceptable[23]. All

JGT extract ligands were docked in the validated grids with AutoDock Vina 1.2.3. For every ligand–receptor pair, Vina returned multiple poses ranked by predicted binding affinity (kcal·mol^{-1}); more negative values indicate stronger predicted binding. The chemically plausible top-scoring pose was retained. JGT ligand was considered competitive when it achieved a Vina score comparable to or more favorable than the erlotinib (reference ligand) benchmark for that same protein and reproduced key interaction motifs in pose overlays (hydrogen bonds, hydrophobics, π-contacts), annotated in PyMOL and BIOVIA Discovery Studio Visualizer[24].

RESULT AND DISCUSSION

Untargeted LC–HRMS of the JGT extract (jaras, Babat Toman shown in **Figure 1a**) revealed ~200 constituents, from which 18 high-priority molecules were curated based on peak area and breast cancer relevance (e.g., naringenin, quercetin, eriodictyol, chlorogenic acid). The 18 prioritized molecules are listed in **Table 1**. The panel is flavonoid/phenolic-rich and consistent with gambier chemotypes reported previously, where catechin-class scaffolds dominate and are frequently linked to redox and kinase-modulatory biology in oncology. Notably, canonical catechin-type flavan-3-ols were not represented among the 18 prioritized constituents listed in **Table 1**; however, a biosynthetically related flavan scaffold was captured as leucodelphinidin (a leucoanthocyanidin/flavan-3,4-diol). Within PASS outputs, predicted activities spanned antineoplastic breast cancer, apoptosis, and chemopreventive terms; the top Pa scores were observed for betulin (anti-breast cancer), echinenone (apoptosis), and mauritianin (chemopreventive), providing hypothesis-level support for downstream targeting and docking analyses. However, compound prioritization for downstream analyses was not based on PASS scores alone, but on an integrated assessment combining network connectivity, target relevance, physicochemical tractability, and ADME/Tox plausibility.

Table 1. LC–HRMS–derived Prioritized Constituents of The JGT Extract with Peak Area and Semi-quantitative Yield

Peak	Compound Name	Molecular Formula	Max. Area	%Yield
1	Kaempferol	$C_{15}H_{10}O_6$	748012757.7	2.10
2	(±)-naringenin	$C_{15}H_{12}O_5$	504981283.2	1.42
3	Quercetin	$C_{15}H_{10}O_7$	504170438.9	1.42
4	Eriodictyol	$C_{15}H_{12}O_6$	58610899.2	0.17
5	Betulin	$C_{30}H_{50}O_2$	40962234.3	0.12
6	Umbelliferone	$C_9H_6O_3$	40502304.7	0.11
7	Hispidulin	$C_{16}H_{12}O_6$	31716649.3	0.09
8	Chlorogenic acid	$C_{16}H_{18}O_9$	30539063.3	0.09
9	Aurasperone c	$C_{31}H_{28}O_{12}$	30259595.2	0.09
10	Plastoquinone	$C_{53}H_{80}O_2$	28292847.5	0.08
11	Hyperoside	$C_{21}H_{20}O_{12}$	26894249.8	0.08
12	Dalpatein	$C_{18}H_{14}O_7$	17508097.7	0.05
13	Morin hydrate	$C_{15}H_{14}O_9$	15189257.2	0.04
14	Echinenone	$C_{40}H_{54}O$	14788843.1	0.04
15	Naringenin chalcone	$C_{15}H_{12}O_5$	14054749.8	0.04
16	Mauritianin	$C_{33}H_{40}O_{19}$	12924310.3	0.04
17	Leucodelphinidin	$C_{15}H_{14}O_8$	11778993.3	0.03
18	Scopoletin	$C_{10}H_8O_4$	9122058.7	0.03

Ligand-based target prediction intersected with a breast cancer gene set yielded 307 candidates for network analysis (**Figure 1b**). The resulting STRING graph contained 307 nodes and 6,559 edges, with a high average node degree (42.7) and significant PPI enrichment ($p < 10^{-16}$), indicating non-random, biologically coherent connectivity among the candidates (**Figure 1e**). Complementing this, a STITCH-based compound–protein overlay mapped representative JGT constituents onto the same network (**Figure 1f**), revealing multi-ligand convergence on high-centrality nodes and directly informing the selection of proteins for docking. This hub-rich topology supports the premise that multiple JGT constituents converge on signaling nodes central to proliferation, survival, inflammation, and stress responses—hallmarks repeatedly implicated in breast cancer progression and resistance.

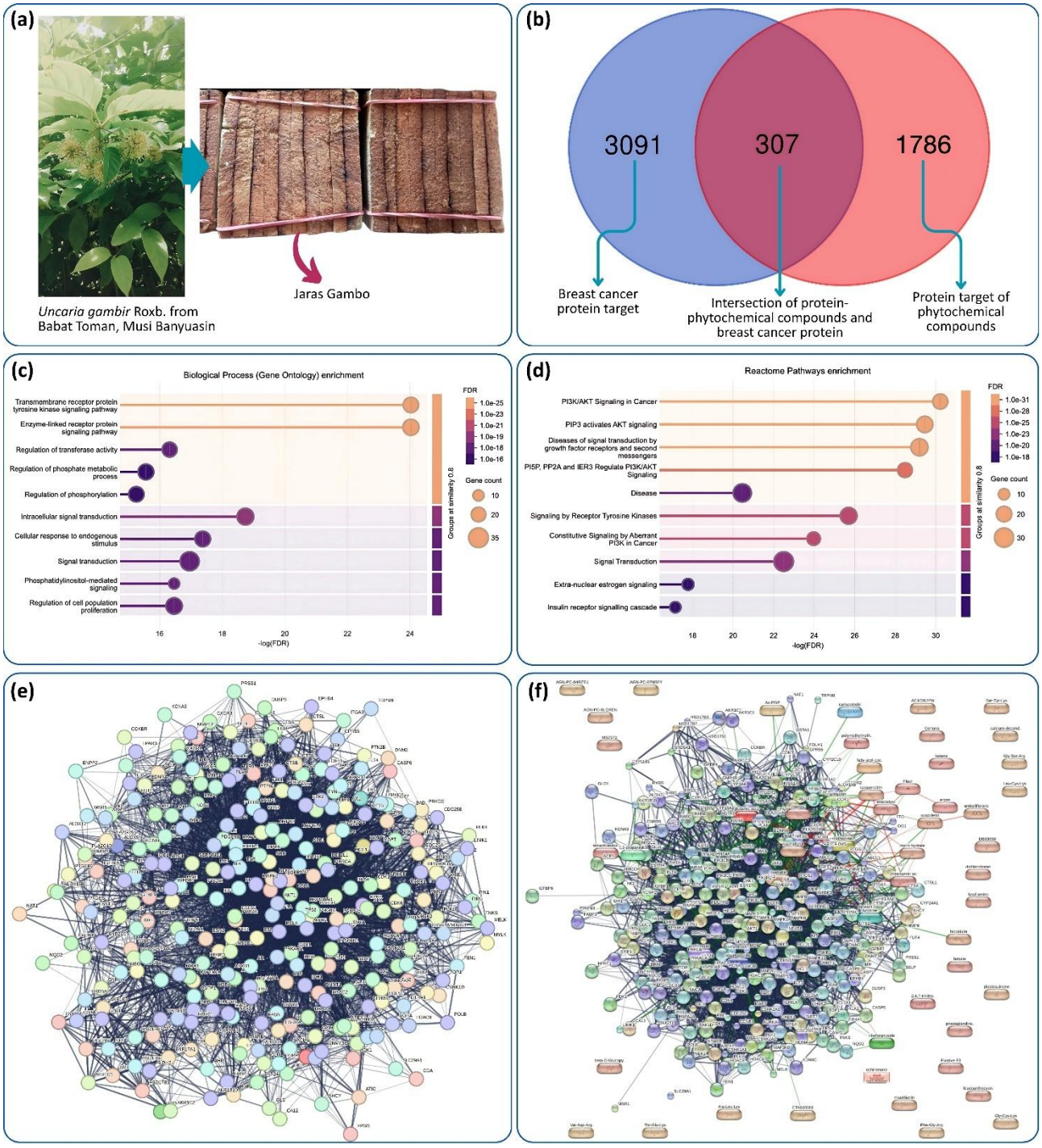

Figure 1. Provenance and network-pharmacology overview of Jaras Gambo Toman (JGT) against breast cancer: (a) Source material: *U. gambir* Roxb. (locally, Gambo) and the processed sap mass (jaras) collected in Babat Toman, Musi Banyuasin (South Sumatra); (b) Target-set intersection (Venn); (c) GO Biological Process enrichment; (d) Reactome pathway enrichment; (e) STRING PPI network; and (f) Compound-protein interactions via STITCH.

Over-representation analysis (on the gene list, not edges) returned coherent signals across ontologies (**Figure 1c–d**). GO Biological Process highlighted receptor-proximal terms such as “transmembrane receptor protein tyrosine kinase (RTK) signaling” and “enzyme-linked receptor protein signaling,” with low FDR values (more significant) that indicate over-representation of JGT-predicted targets in these processes. In this context, “transmembrane receptor protein tyrosine kinase signaling” points to ligand-driven activation of membrane receptors such as EGFR that initiate downstream cascades promoting proliferation and survival. Meanwhile, the broader “enzyme-linked receptor protein signaling” term captures these receptors together with other membrane systems that signal through associated kinases[25–28].

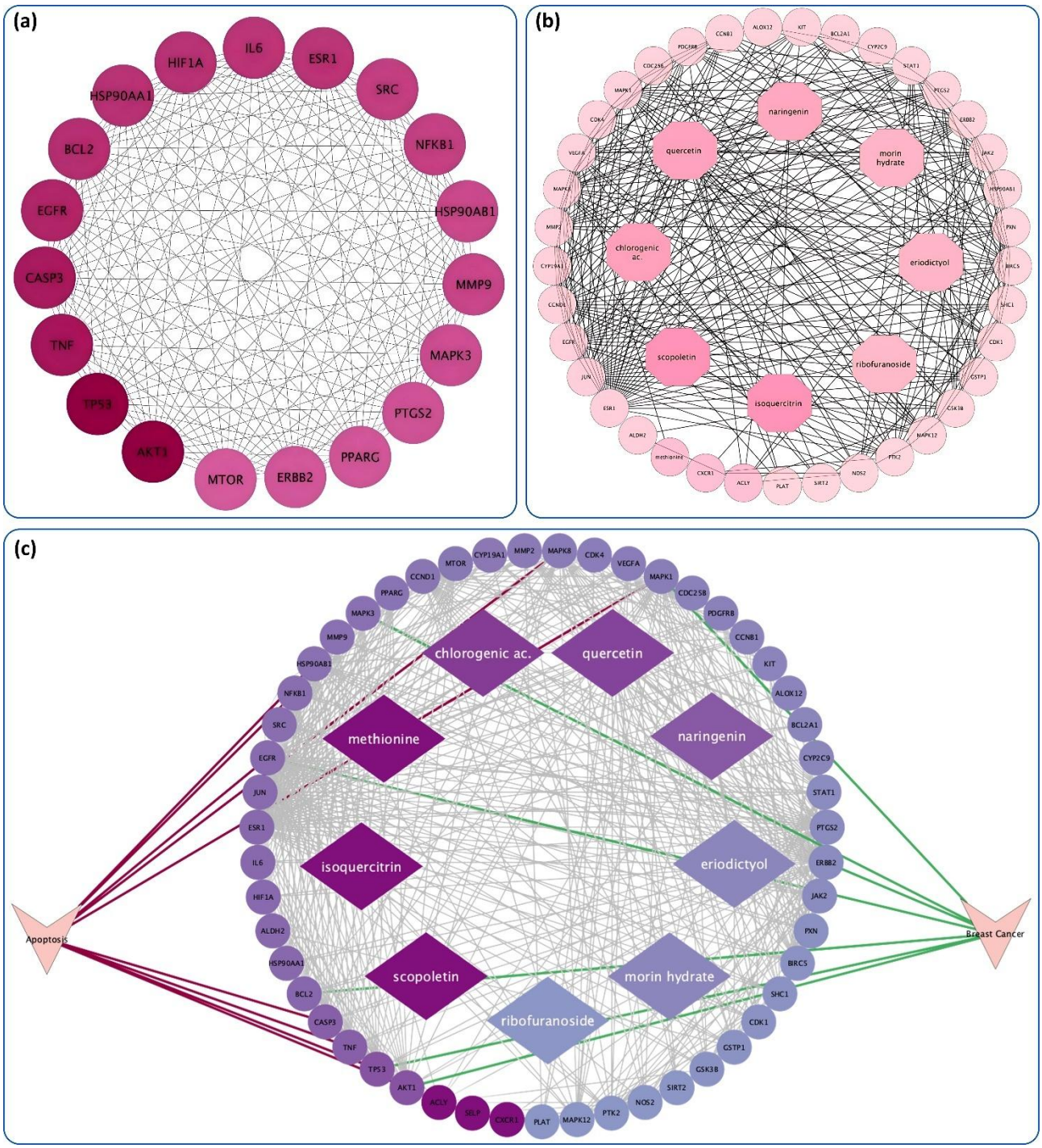

Figure 2. Network pharmacology of the JGT extract: (a) PPI visualized in Cytoscape; (b) CPI network linking representative JGT phytochemicals (inner nodes) to breast cancer–relevant targets (outer ring); and (c) Integrated compound–target–phenotype map with phenotype anchors (apoptosis, breast cancer) showing convergence of JGT constituents on hub-rich signaling.

Consistently, Reactome emphasized PI3K/AKT signaling modules (e.g., “PIP3 activates AKT signaling,” “diseases of signal transduction by growth-factor receptors”), indicating that growth-factor inputs converge on lipid-signaling events that activate AKT and support anabolic growth, cell-cycle progression, and reduced apoptosis[29,30]. The prominence of AKT1 and EGFR as network hubs alongside the apoptosis regulators TP53 and BCL2, therefore, aligns with these enriched terms, linking receptor-level signals to survival pathways and programmed cell death control in breast cancer[31].

From our network pharmacology analysis (**Figure 2a-c**), eight high-connectivity nodes were prioritized—chlorogenic acid, eriodictyol, isoquercitrin, morin hydrate, naringenin, quercetin, ribofuranoside, and scopoletin. These compounds were consequently advanced for physicochemical and drug-likeness profiling. Physicochemical properties

were predicted using the MolSoft web platform and SwissADME. Evaluation followed Lipinski's Rule of Five, encompassing molecular weight (≤500 g/mol), lipophilicity (log P ≤5), hydrogen-bond donors (≤5), hydrogen-bond acceptors (≤10), rotatable bonds (≤10), and molar refractivity (30–140)[32]. The predicted parameters for each compound are summarized in **Table 2**.

Table 2. Physicochemical Profile and Lipinski Assessment of Prioritized JGT Constituents (Core Ro5 and General Properties)

Parameters		Chlorogenic Acid	Eriodictyol	Iso-quercitrin	Morin hydrate	Naringenin	Quercetin	Ribo-furanoside	Scopoletin
Lipinski's Parameters	Size (Molecular weight; g/mol)	354.31	288.25	464.38	338.27	272.25	302.24	150.13	192.17
	Lipophilicity Log P (XLOGP3)	-0.42	2.02	0.36	1.76	2.82	1.54	-2.32	1.53
	Insolubility (Log S; ESOL)	-1.62	-3.26	-2.97	-3.22	-3.55	-3.16	0.76	-2.46
	Polarity (Å²)	164.75	107.22	210.51	111.13	97.99	131.36	90.15	59.67
	Insaturation (Fraction Csp3)	0.38	0.13	0.29	0.00	0.00	0.00	1.00	0.10
	Rotatable bonds	5.00	1.00	5.00	1.00	3.00	1.00	1.00	1.00
	H-bond donors	6.00	4.00	8.00	4.00	4.00	5.00	4.00	1.00
	H-bond acceptors	9.00	6.00	12.00	6.00	5.00	7.00	5.00	4.00
	Molar refractivity	83.50	73.59	110.16	76.01	74.34	78.03	29.77	51.00
	Lipinski status	No; 2 violations	Yes; 0 violation	No; 2 violations	Yes; 0 violation	Yes; 0 violation	Yes; 0 violation	No; 2 violations	Yes; 0 violation
General Properties	Boiling Point	428.98	453.76	643.34	502.75	453.14	507.2	330.62	338.64
	Hydration Free Energy	-9.74	-11.27	-4.30	-10.94	-13.29	-11.02	-22.59	-9.85
	Log(D) at pH=7.4	-1.53	1.97	-0.02	1.79	2.65	1.39	-2.39	1.58
	Log(Vapor Pressure)	-13.27	-8.26	-11.78	-7.78	-7.52	-8.26	-9.17	-4.59
	Melting Point	199.24	236.82	209.83	309.78	211.97	327.42	150.85	198.88
	pKa Acid	2.87	6.08	5.39	6.76	6.32	6.94	8.96	6.42
	pKa Basic	7.34	7.60	8.16	7.00	7.23	7.18	2.15	3.96

Five of the eight phytochemicals met Lipinski's expectations. All compounds were within the ≤500 g/mol molecular-weight range, supporting the possibility of passive transcellular diffusion. Eriodictyol, morin hydrate, naringenin, quercetin, and scopoletin also satisfied the logP (≤5) and hydrogen-bond donor/acceptor limits, indicative of a polarity–lipophilicity balance compatible with oral absorption. Rotatable-bond counts pointed to restrained conformational mobility—helpful for reducing entropic penalties during target engagement—while most molecules fell inside the recommended molar-refractivity corridor (30–140), a proxy for polarizability and noncovalent interaction strength. An outlier was ribofuranoside (MR = 29.77), whose sub-threshold polarizability implies weaker dispersive contacts and, by extension, less favorable membrane partitioning. Even so, and in line with criteria proposed by Chander *et al.* (2017), chlorogenic acid, isoquercitrin, and ribofuranoside remain viable early-stage leads, albeit with anticipated permeability liabilities that may necessitate aglycone liberation, prodrug design, or formulation-enabled transport[33].

The ADME prediction (**Table 3**) reveals that the absorption of naringenin and eriodictyol show the most favorable proxies (Caco-2 logPapp least negative; human intestinal absorption ~0.93–0.94; oral bioavailability estimates highest in the group), whereas isoquercitrin is consistently poor (Caco-2 ~−6.3; HIA ~0.22; OBA ≤0.21), coherent with its glycosidic polarity and P-gp substrate signal. Quercetin sits intermediate (HIA ~0.87; modest P-gp substrate probability), compatible with known variability in its oral exposure. Distribution parameters also separate the aglycones: naringenin is the only compound here with a meaningful BBB probability (≈0.21), while others trend near zero, and protein binding/fraction unbound values indicate generally moderate to high plasma binding for the flavonoid core. Metabolism

flags are concentrated in the polyphenols: quercetin, naringenin, and morin hydrate show higher probabilities of CYP1A2/2C9/3A4 inhibition than chlorogenic acid or isoquercitrin, foreshadowing DDI risks that will matter only if exposures are sufficient. On excretion, isoquercitrin and eriodictyol exhibit the highest predicted clearance, suggesting shorter residence unless compensated by input rate or formulation; naringenin and quercetin are more moderate, with half-life surrogates that are not obviously prohibitive.

Table 3. In silico ADME Projections for Prioritized JGT Constituents

	Parameters	Chlorogenic acid	Eriodictyol	Iso-quercitrin	Morin hydrate	Naringenin	Quercetin	Ribo-furanoside	Scopoletin
Absorption	Caco-2 (logPapp)	-6.270	-5.300	-6.290	-5.800	-4.940	-5.800	-5.100	-4.510
	Human OBA 20%	0.339	0.409	0.206	0.365	0.475	0.419	0.675	0.730
	Human Intestinal Abs.	0.790	0.937	0.215	0.842	0.934	0.866	0.901	0.993
	MD Canine Kidney	-4.030	-5.050	-5.800	-5.360	-4.910	-5.360	-2.560	-4.190
	Human OBA 50%	0.384	0.529	0.193	0.499	0.527	0.474	0.357	0.593
	P-Glycoprotein Inhibitor	0.000	0.000	0.302	0.004	0.001	0.001	0.000	0.035
	P-Glycoprotein Substrate	0.353	0.155	0.449	0.151	0.101	0.180	0.123	0.073
Distribution	BBB (Central Nervous System)	-3.810	-2.850	-4.210	-3.170	-2.340	-3.120	-3.560	-2.350
	Blood-Brain Barrier	0.002	0.009	0.000	0.002	0.209	0.001	0.839	0.453
	Fraction Unbound	0.600	0.880	0.830	0.780	0.720	0.800	0.330	0.920
	Plasma Protein Binding	-0.600	66.35	81.240	95.13	60.04	97.17	19.67	55.78
	VDss	0.420	0.610	0.900	0.160	0.640	0.140	0.220	0.190
Metabolism	BC Res. Protein	0.019	0.167	0.122	0.655	0.397	0.597	0.018	0.339
	CYP 1A2 Inhib.	0.085	0.771	0.270	0.948	0.898	0.974	0.001	0.852
	CYP 1A2 Subs.	0.001	0.500	0.006	0.152	0.344	0.175	0.042	0.564
	CYP 2C19 I	0.000	0.582	0.000	0.252	0.523	0.136	0.010	0.099
	CYP 2C19 S	0.185	0.494	0.174	0.32	0.429	0.297	0.279	0.462
	CYP 2C9 I	0.000	0.329	0.034	0.896	0.533	0.738	0.001	0.199
	CYP 2C9 S	0.031	0.880	0.017	0.328	0.597	0.122	0.000	1.000
	CYP 2D6 I	0.000	0.063	0.000	0.046	0.444	0.02	0.000	0.001
	CYP 2D6 S	0.167	0.262	0.165	0.183	0.203	0.265	0.353	0.469
	CYP 3A4 I	0.027	0.782	0.042	0.648	0.947	0.488	0.008	0.083
	CYP 3A4 S	0.000	0.006	0.000	0.000	0.009	0.000	0.003	0.441
	OATP1B1	0.267	0.165	0.193	0.347	0.240	0.295	0.003	0.022
	OATP1B3	0.079	0.072	0.206	0.106	0.103	0.100	0.025	0.032
Excretion	Clearance	5.590	13.100	13.650	7.880	6.570	8.910	2.080	7.030
	Organic Cation Transporter 2	0.002	0.266	0.470	0.475	0.163	0.453	0.003	0.027
	Half-Life of Drug	0.759	0.294	0.324	0.317	0.433	0.326	0.871	0.247

Information:

Caco-2 (logPapp): apparent permeability proxy
Human OBA: probability of oral bioavailability
HIA: human intestinal absorption
BBB / CNS: blood–brain barrier likelihood
VDss: steady-state volume of distribution
CYP (1A2, 2C19, 2C9, 2D6, 3A4) I/S: probability as inhibitor/substrate for each isoform
OATP1B1/1B3: hepatic/renal transporter interaction probabilities
Units: unless stated otherwise, dimensionless entries denote probabilities (0–1)

Based on the toxicity predictions summarized in **Table 4**, the JGT constituents display a differentiated risk profile that guides compound prioritization for follow-up assays. Naringenin appeared to show the most favorable predicted safety profile (low hERG and Ames), making it a suitable initial candidate for cellular follow-up studies. Quercetin showed higher predicted hERG and liver-injury propensities and should be used under tighter exposure with early Ames/cardiotoxicity counterscreens. Isoquercitrin presents an elevated Ames flag and poor biodegradation, yet is likely exposure-limited by weak absorption/rapid clearance; if advanced as the kinase-pocket lead, pair it with explicit genotoxicity assays and metabolism controls. Chlorogenic acid appears benign on mutagenicity/hERG but remains delivery-constrained by polarity; eriodictyol mirrors naringenin's absorption but with higher hERG/nuclear-receptor flags; and morin hydrate resembles quercetin's risk posture.

Table 4. In silico Toxicity Predictions for Prioritized JGT Constituents

Parameters	Chlorogenic Acid	Eriodictyol	Iso-quercitrin	Morin hydrate	Naringenin	Quercetin	Ribo-furanoside	Scopo-letin
AMES Mutagenesis	0.000	0.042	0.998	0.200	0.005	0.282	0.201	0.114
Avian	0.000	0.024	0.002	0.039	0.025	0.053	0.047	0.336
Bee	0.390	0.642	0.474	0.506	0.420	0.448	0.764	0.297
Bioconcentration Factor	-1.690	0.170	-2.480	1.040	1.000	0.380	-1.450	1.360
Biodegradation	0.930	0.076	0.016	0.001	0.062	0.001	0.901	0.657
Carcinogenesis	0.046	0.461	0.016	0.311	0.433	0.288	0.460	0.273
Crustacean	0.002	0.390	0.110	0.820	0.533	0.728	0.004	0.472
Liver Injury I (DILI)	0.327	0.643	0.525	0.769	0.701	0.775	0.457	0.695
Maximum Tolerated Dose	0.480	1.110	1.150	1.230	1.02	1.180	2.580	1.450
Liver Injury II	0.482	0.499	0.663	0.626	0.468	0.615	0.337	0.567
hERG Blockers	0.000	0.261	0.065	0.415	0.010	0.469	0.073	0.028
Daphnia Magna	4.630	4.690	5.060	5.100	4.360	5.120	2.960	4.410
Micronucleus	0.994	0.985	1.000	0.998	0.953	0.998	0.067	0.687
NR-AhR	0.007	0.780	0.538	0.842	0.783	0.824	0.000	0.575
NR-AR	0.111	0.066	0.215	0.060	0.060	0.079	0.012	0.006
NR-AR-LBD	0.037	0.003	0.018	0.007	0.003	0.011	0.017	0.014
NR-Aromatase	0.000	0.085	0.000	0.004	0.010	0.001	0.000	0.000
NR-ER	0.106	0.539	0.179	0.563	0.835	0.512	0.050	0.118
NR-ER-LBD	0.011	0.558	0.011	0.194	0.750	0.364	0.013	0.014
NR-GR	0.176	0.198	0.024	0.262	0.545	0.273	0.032	0.253
NR-PPAR-gamma	0.000	0.008	0.000	0.001	0.007	0.001	0.005	0.034
NR-TR	0.004	0.432	0.002	0.186	0.906	0.036	0.000	0.028
T. Pyriformis	2.680	4.350	-122.350	2.920	4.610	3.100	-1.250	3.480
Rat (Acute)	1.910	2.180	2.420	2.490	2.150	2.500	0.920	1.880
Rat (Chronic Oral)	3.300	3.000	3.860	3.560	3.110	3.460	2.570	2.080
Fathead Minnow	3.800	4.120	3.850	3.910	4.340	3.940	1.160	4.020
Respiratory Disease	0.956	0.769	0.074	0.025	0.116	0.086	0.023	0.128
SR-ARE	0.078	0.421	0.422	0.436	0.861	0.554	0.026	0.059
SR-ATAD5	0.000	0.010	0.002	0.003	0.101	0.006	0.000	0.193
SR-HSE	0.001	0.055	0.000	0.004	0.139	0.003	0.001	0.075
SR-MMP	0.000	0.969	0.006	0.966	0.997	0.944	0.000	0.045
SR-p53	0.000	0.003	0.013	0.079	0.533	0.032	0.006	0.978

Information:
AMES: mutagenicity classifier
DILI: drug-induced liver injury risk
hERG: potassium-channel blockade proxy (cardiotoxicity)
NR-(ER/AR/GR/PPARγ/TR/AhR): nuclear-receptor activity alerts
SR-(ARE/ATAD5/HSE/MMP/p53): stress-response pathway alerts.
Units: unless stated otherwise, dimensionless entries denote probabilities (0–1)

Network pharmacology analysis revealed a tightly interconnected core of disease-relevant proteins—AKT1, TNF, EGFR, TP53, and BCL2. Aberrations converging on EGFR–PI3K/AKT signaling, p53-dependent genome surveillance, mitochondrial apoptosis, and NF-κB–driven inflammation place AKT1, EGFR, TP53, BCL2, and TNF at the heart of breast cancer biology and therapy. EGFR overexpression and activation channel proliferative cues into AKT1, a central effector that integrates growth and metabolic control and underlies resistance—clinically mirrored by benefits of PI3K/AKT-targeted agents in biomarker-selected disease[34]. Conversely, TP53 loss disables DNA-damage checkpoints and accelerates genomic instability, while BCL2 sets the mitochondrial threshold for apoptosis, shaping responses to endocrine and cytotoxic regimens[35]. TNF sustains a pro-tumor inflammatory milieu via NF-κB and crosstalks with EGFR–AKT to promote invasion, immune evasion, and drug tolerance[36,37]. Together, these nodes delineate a coherent, actionable axis, justifying combination strategies that align receptor blockade with PI3K/AKT inhibition, apoptosis priming, and inflammation control across relevant molecular subtypes.

Docking across five hub proteins (AKT1, BCL2, EGFR, TNF, TP53) used erlotinib as a computational comparator in each pocket to standardize scoring and pose assessment (**Table 5**). Several JGT extract ligands were competitive or superior on a per-target basis when judged by AutoDock Vina scores (kcal·mol^{-1}, more negative indicates stronger predicted binding). In the EGFR kinase pocket, isoquercitrin gave the most favorable score (−8.748), with eriodictyol (−8.523) and quercetin (−8.335) also outperforming erlotinib (−6.883). An in silico/in vitro study on MDA-MB-231 likewise prioritized isoquercitrin as a high-connectivity hit and a top EGFR-directed ligand, reproducing hinge/catalytic-

loop contacts at MET793 and ASP800 and maintaining a stable complex over 200-ns MD, comparable to lapatinib[38]. Despite different engines and scoring schemes (AutoDock Vina here vs. Glide/MM-GBSA there), both studies elevate EGFR as the privileged target and isoquercitrin as the best-in-class ligand—directly mirroring our EGFR result and reinforcing its robustness.

Table 5. Docking Binding Affinities of JGT Constituents Across Five Breast Cancer-Relevant Hubs

Ligand compound	Binding Affinity (kcal·mol^{-1})				
	AKT1	BCL2	EGFR	TNF	TP53
Chlorogenic acid	−5.160 †	−6.342 †	−7.006 †	−5.875 †	−8.589 †
Eriodictyol	−5.084 †	−6.440 †	−8.523 †	−6.344 †	−8.358 †
Isoquercitrin	**−5.538** †	−6.596 †	**−8.748** †	−5.827 †	**−8.975** †
Morin hydrate	−5.491 †	−6.455 †	−8.149 †	−5.812 †	−7.831 †
Naringenin	−5.154 †	**−6.838** †	−8.227 †	**−6.444** †	−8.080 †
Quercetin	−5.021 †	−6.397 †	−8.335 †	−5.828 †	−8.197 †
Ribofuranoside	−3.924	−3.296	−4.390	−3.521	−4.963
Scopoletin	−4.350	−5.164	−5.868	−4.805	−6.897
Erlotinib (reference)	−4.749	−6.224	−6.883	−5.546	−7.611

Information:
Erlotinib: the reference (comparator) ligand in each pocket
Bold: lowest (most negative) binding affinity within a column (best predicted binder for that target)
† = stronger (more negative) than the erlotinib reference for the same target

For the anti-apoptotic BCL2, naringenin surpassed the reference (−6.838 vs −6.224), and a similar advantage was observed in TNF (−6.444 vs −5.546). This pattern is concordant with prior mechanistic data: naringenin downregulates BCL2 in the MCF-7 cell line and engages executioner caspases while concurrently suppressing survival signaling (NF-κB/pAkt/PI3K), thereby priming breast cancer cells for apoptosis, and it modulates the TNF axis in a context-dependent manner[39], supporting our docking signals on BCL2 and TNF as biologically plausible. In TP53, chlorogenic acid showed a markedly stronger prediction than erlotinib (−8.589 vs −7.611). Finally, in AKT1, isoquercitrin again edged the benchmark (−5.538 vs −4.749). Collectively, these head-to-head comparisons indicate that multiple JGT constituents can plausibly occupy functionally relevant pockets across five hubs with affinities that meet or exceed the reference baseline for the same targets.

Figure 3 visualizes chemically consistent poses across all hubs, with binding driven by hydrogen bonds (green) and aromatic contacts (pink = π–π stacked; light-pink = π–alkyl; purple = π–σ). In AKT1–isoquercitrin (a), the polyhydroxylated flavonol engages a polar ridge through multiple hydrogen bonds (green) to residues such as Glu17, Asn53, Lys14, and Arg86, and limited π–alkyl contacts with aliphatic side chains (e.g., Leu52). In BCL2–naringenin (b), the chromanone core stacks against Phe63 (π–π) and packs against Leu96 (π– σ), while directional H-bonds to Glu95 and Arg105 secure the pose in the anti-apoptotic groove. The EGFR–isoquercitrin (c) complex shows the densest lattice: H-bonds to Glu738, Lys721, Thr766, Arg817, Ala719, and Asp831 are reinforced by hydrophobic/π contacts with Ala719, Val702, Leu694, Leu820, and Phe699, explaining the top Vina score in this pocket. In TNF–naringenin (d), a shallow-cleft pose is stabilized by an H-bond to Ser60 and His15, with auxiliary π–type contacts to Tyr59 and Leu120 that maintain residency despite the limited depth of the cytokine interface. Finally, TP53–chlorogenic acid (e) leverages catechol–carboxylate polarity to form two discrete H-bonds with Glu228 and Asn265, reinforced by an additional hydrogen bond to His297, π–π stacking with Trp352, π–σ contact to Ala226, and a π–alkyl contact to Ile223. Collectively, complexes that couple multi-point H-bonding to well-placed aromatic packing exhibit superior desolvation and shape complementarity, mirroring the observed docking hierarchy and supporting a polypharmacologic mechanism spanning survival (PI3K/AKT), apoptosis control (BCL2/TP53), and inflammation-related signaling (TNF/NF-κB).

Across JGT-relevant chemotypes, convergent evidence supports a breast cancer–oriented rationale that spans phenolic acids and multiple flavonoid subclasses, but this evidence is most appropriately interpreted at the level of shared pathway coverage by a multicompound matrix, rather than as a one-to-one transfer of single-compound mechanisms to the crude extract. Literature on representative constituents detected in JGT—such as chlorogenic acid, quercetin and its glycosides (e.g., isoquercitrin), naringenin, scopoletin, and morin hydrate—consistently reports anti-proliferative and pro-apoptotic tendencies, while also highlighting important limitations related to bioavailability[40-47]. Consequently, the compound-specific mechanisms discussed here should be regarded as mechanistic signposts that inform extract-level hypotheses, not as direct proof that JGT reproduces each isolated compound's activity. In addition, the present study relies on an in silico prioritization pipeline (target prediction, enrichment, and docking), which

supports target plausibility but does not establish causality, dose–response relationships, or the active fractions responsible for the predicted activities.

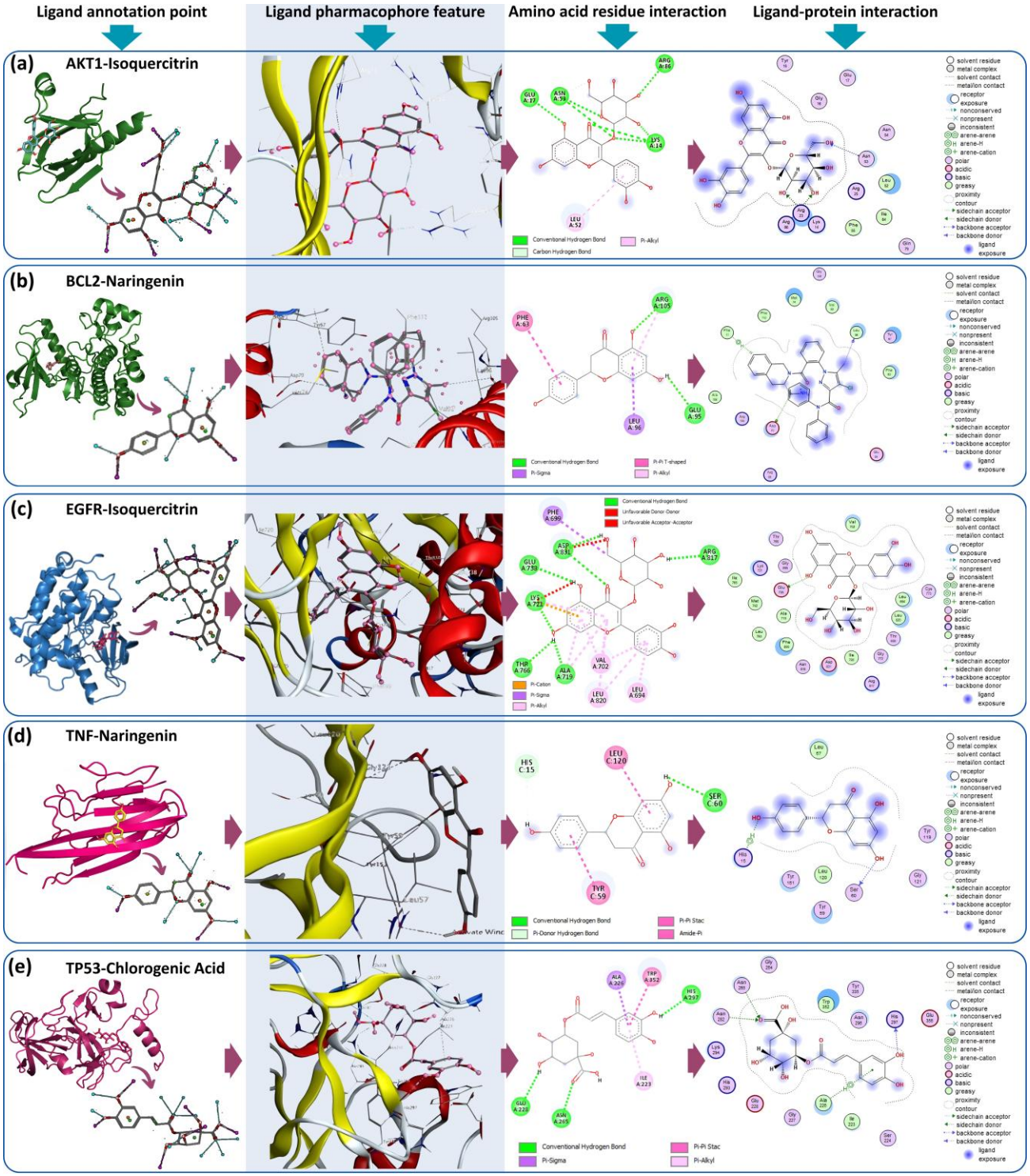

Figure 3. Representative docked complexes and interaction fingerprints of prioritized JGT constituents: (a) AKT1–isoquercitrin; (b) BCL2–naringenin; (c) EGFR–isoquercitrin; (d) TNF–naringenin; and (e) TP53–chlorogenic acid.

Future work should therefore focus on bridging this inference-to-evidence gap through: (i) extract standardization with targeted LC–MS/MS quantification of selected marker compounds to ensure batch-to-batch reproducibility; (ii) bioactivity-guided fractionation coupled to iterative docking/network updates to localize activity to specific fractions; (iii) reconstitution and interaction testing (single compounds vs. defined mixtures vs. whole extract) to determine whether observed effects reflect synergy, additivity, or antagonism; and (iv) orthogonal biological validation in breast cancer subtypes (e.g., ER+, HER2+, and TNBC) using functional assays (viability, apoptosis, migration/EMT) and pathway readouts that directly test predicted nodes (e.g., phospho-AKT/ERK, NF-κB activity,

TP53/BCL2/TNF–EGFR signaling). Extension to ADME/metabolite profiling and in vivo efficacy/safety will be essential to establish translational relevance and define a realistic therapeutic window.

Limitation

Several limitations should be acknowledged when interpreting the present findings. First, the identification of bioactive constituents and their putative anti-breast cancer relevance was derived from LC–HRMS profiling combined with network pharmacology and molecular docking. Although this integrated strategy is valuable for hypothesis generation, it remains inferential and cannot, on its own, demonstrate biological activity in a physiological setting. Second, the predicted target–pathway relationships and binding profiles rely heavily on database-based annotations and computational modeling, both of which inevitably simplify the biological complexity of breast cancer, including tumor heterogeneity, pharmacokinetic behavior, bioavailability, and context-dependent intracellular responses. Third, while the docking analysis supports the plausibility of compound–target interactions at the molecular level, it does not provide direct evidence of therapeutic efficacy, target selectivity, or safety. These aspects require confirmation through experimental investigation. Even so, the present study offers a useful mechanistic basis for understanding how Uncaria gambir–derived constituents may act on multiple breast cancer–related proteins and signaling pathways. In this regard, the findings help define a rational starting point for subsequent in vitro and in vivo studies aimed at validating the cytotoxic, antiproliferative, and pro-apoptotic potential of the prioritized compounds, while also informing the future development of plant-derived multi-target candidates for breast cancer research.

CONCLUSION

Jaras Gambo Toman (JGT) extract shows promise as a complementary candidate in breast cancer research. The active compounds identified in the extract exhibited multi-target in silico interactions with several breast cancer-related proteins, suggesting a potential polypharmacological profile. Such a profile may be relevant for addressing therapeutic resistance, although this implication remains preliminary. Furthermore, the prioritized compounds demonstrated comparable in silico binding affinity profiles to erlotinib across selected targets. However, these in silico findings do not by themselves predict comparable biological responses under experimental or clinical conditions. Therefore, further in vitro and in vivo studies are needed to validate the anticancer activity, safety, and therapeutic potential of JGT extract.

FUNDING

This study was self-funded by the authors and did not involve external financial assistance.

ACKNOWLEDGMENTS

We would like to thank all those who contributed to this research, especially the Department of Pharmacy, Faculty of Mathematics and Natural Sciences, Universitas Sriwijaya, for supporting the continuity of this research.

GENERATIVE AI DISCLOSURE STATEMENT

During manuscript development, the authors utilized ChatGPT (OpenAI) as an AI-assisted tool to support language editing, grammar correction, sentence refinement, and improvement of readability and clarity. All outputs were subsequently assessed, revised, and validated by the authors, who retain full responsibility for the scientific content, interpretation, and integrity of the publication.

AUTHOR CONTRIBUTION STATEMENT

Rafiqah Nur Viviani: Formal analysis, Validation, Writing—Review and Editing; **Nathasya Shasykirana Mahendra**: Investigation, Data curation; **Shaum Shiyan**: Conceptualization, Methodology, Supervision, Funding acquisition; **Galih Pratiwi**: Software, Visualization.

CONFLICT OF INTEREST

The authors declare no conflict of interest.

REFERENCES

1. Łukasiewicz S, Czeczelewski M, Forma A, Baj J, Sitarz R, Stanisławek A. Breast cancer—epidemiology, risk factors, classification, prognostic markers, and current treatment strategies—An updated review. *Cancers (Basel)*. 2021;13(17). doi:10.3390/cancers13174287
2. Guo L, Kong D, Liu J, et al. Breast cancer heterogeneity and its implication in personalized precision therapy. *Exp Hematol Oncol*. 2023;12(1). doi:10.1186/s40164-022-00363-1
3. Henry NL, Kim S, Hays RD, et al. Toxicity Index, patient-reported outcomes, and persistence of breast cancer chemotherapy-associated side effects in NRG Oncology/NSABP B-30. *NPJ Breast Cancer*. 2022;8(1). doi:10.1038/s41523-022-00489-9
4. Pedersen RN, Esen BÖ, Mellemkjær L, et al. The Incidence of breast cancer recurrence 10-32 years after primary diagnosis. *J Natl Cancer Inst*. 2022;114(3):391-399. doi:10.1093/jnci/djab202
5. Rosso R, D'Alonzo M, Bounous VE, et al. Adherence to adjuvant endocrine therapy in breast cancer patients. *Current Oncology*. 2023;30(2):1461-1472. doi:10.3390/curroncol30020112
6. Al Khalily IA, Megantara S, Aulifa DL. Targeting molecular pathways in breast cancer using plant-derived bioactive compounds: A comprehensive review. *J Exp Pharmacol*. 2025;17:375-401. doi:10.2147/JEP.S528132
7. Sohel M, Aktar S, Biswas P, et al. Exploring the anti-cancer potential of dietary phytochemicals for the patients with breast cancer: A comprehensive review. *Cancer Med*. 2023;12(13):14556-14583. doi:10.1002/cam4.5984
8. Munggari IP, Kurnia D, Deawati Y, Julaeha E. Current research of phytochemical, medicinal and non-medicinal uses of *Uncaria gambir* Roxb.: A review. *Molecules*. 2022;27(19). doi:10.3390/molecules27196551
9. Rahmaddiansyah R, Hasani S, Zikrah AA, Arisanty D. The effect of gambier catechin isolate on cervical cancer cell death (hela cell lines). *Open Access Maced J Med Sci*. 2022;10(B):1293-1297. doi:10.3889/oamjms.2022.8779
10. Wardana AP, Aminah NS, Kristanti AN, et al. Nano *Uncaria gambir* as chemopreventive agent against breast cancer. *Int J Nanomedicine*. 2023;18:4471-4484. doi:10.2147/IJN.S403385
11. Gao J, Wang N, Song W, Yuan Y, Teng Y, Liu Z. Mechanisms underlying the synergistic effects of chuanxiong combined with Chishao on treating acute lung injury based on network pharmacology and molecular docking combined with preclinical evaluation. *J Ethnopharmacol*. 2024;325:117862. doi:https://doi.org/10.1016/j.jep.2024.117862
12. Lee WY, Lee CY, Kim YS, Kim CE. The methodological trends of traditional herbal medicine employing network pharmacology. *Biomolecules*. 2019;9(8). doi:10.3390/biom9080362
13. Li L, Kar S. Leveraging network pharmacology for drug discovery: Integrative approaches and emerging insights. *Med Drug Discov*. 2025;27. doi:10.1016/j.medidd.2025.100220
14. Ferreira LLG, Andricopulo AD. ADMET modeling approaches in drug discovery. *Drug Discov Today*. 2019;24(5):1157-1165. doi:10.1016/j.drudis.2019.03.015
15. Muhammed MT, Aki-Yalcin E. Molecular docking: Principles, advances, and its applications in drug discovery. *Lett Drug Des Discov*. 2024;21(3):480-495. doi:https://doi.org/10.2174/1570180819666220922103109
16. Adelusi TI, Oyedele AQK, Boyenle ID, et al. Molecular modeling in drug discovery. *Inform Med Unlocked*. 2022;29. doi:10.1016/j.imu.2022.100880
17. Aries Seka O, Kiagus Ahmad Roni I, Elfidiah I, Author C. Optimizing the effect of gambir sap extract as an organic inhibitor to reduce scale formation at pertamina hulu energi (OK/RT) Peninjauan District, OKU Regency. *Int j adv multidisc res stud*. 2023;3(5):73-77.
18. Kızıltaş H, Bingol Z, Gören AC, et al. LC-HRMS profiling and antidiabetic, anticholinergic, and antioxidant activities of aerial parts of kınkor (*Ferulago stellata*). *Molecules*. 2021;26(9). doi:10.3390/molecules26092469
19. Filimonov DA, Rudik A V., Dmitriev A V., Poroikov V V. Computer-aided estimation of biological activity profiles of drug-like compounds taking into account their metabolism in human body. *Int J Mol Sci*. 2020;21(20):1-13. doi:10.3390/ijms21207492
20. Nugraha SE, Marianne M, Syahputra RA, et al. Efficacy of *Carica papaya* leaves extract for treating thrombocytopenia: An in silico and in vivo study in rat model. *Adv Anim Vet Sci*. 2024;12(7):1325-1334. doi:10.17582/journal.aavs/2024/12.7.1325.1334
21. Astuti PDY, Fadilah F, Promsai S, Bahtiar A. Integrating molecular docking and molecular dynamics simulations to evaluate active compounds of Hibiscus schizopetalus for obesity. *J Appl Pharm Sci*. 2024;14(4):176-187. doi:10.7324/JAPS.2024.158550
22. Desa S, Osman A, Hyslop R. In silico assessment of drug-like properties of phytocannabinoids in *Cannabis sativa*. *EJSMT*. 2017;4(2):1-7. doi:10.37134/ejsmt.vol4.2.1.2017

23. Ramírez D, Caballero J. Is it reliable to take the molecular docking top scoring position as the best solution without considering available structural data? *Molecules*. 2018;23(5). doi:10.3390/molecules23051038
24. Purnama A, Rizki D, Qanita I, et al. Molecular docking investigation of calotropone as a potential natural therapeutic agent against pancreatic cancer. *J Adv Pharm Technol Res*. 2022;13(1):44-49. doi:10.4103/japtr.japtr_143_21
25. Slika H, Mansour H, Wehbe N, et al. Therapeutic potential of flavonoids in cancer: ROS-mediated mechanisms. *Biomedicine and Pharmacotherapy*. 2022;146. doi:10.1016/j.biopha.2021.112442
26. Qi Y. Receptor tyrosine kinases in breast cancer treatment: unraveling the potential. *Am J Cancer Res*. 2024;14(9):4172-4196. doi:10.62347/kivs3169
27. Pottier C, Fresnais M, Gilon M, Jérusalem G, Longuespée R, Sounni NE. Tyrosine kinase inhibitors in cancer: Breakthrough and challenges of targeted therapy. *Cancers (Basel)*. 2020;12(3). doi:10.3390/cancers12030731
28. Abotaleb M, Liskova A, Kubatka P, Büsselberg D. Therapeutic potential of plant phenolic acids in the treatment of cancer. *Biomolecules*. 2020;10(2). doi:10.3390/biom10020221
29. Huang D, Yang J, Zhang Q, et al. Design, synthesis, and biological evaluation of 2,4-dimorpholinopyrimidine-5-carbonitrile derivatives as orally bioavailable PI3K inhibitors. *Front Pharmacol*. 2024;15. doi:10.3389/fphar.2024.1467028
30. Suhail M, AlZahrani WM, Shakil S, et al. Analysis of some flavonoids for inhibitory mechanism against cancer target phosphatidylinositol 3-kinase (PI3K) using computational tool. *Front Pharmacol*. 2023;14. doi:10.3389/fphar.2023.1236173
31. Silva GB da, Rocha KG, Bagatini MD, Kempka AP. Anticancer properties of phenolic acids and cell death signaling pathways: A 20-year bibliometric analysis (2003–2023). *Food Biosci*. 2025;63. doi:10.1016/j.fbio.2024.105741
32. Guan L, Yang H, Cai Y, et al. ADMET-score – a comprehensive scoring function for evaluation of chemical drug-likeness. *Med Chem Commun*. 2019;10(1):148-157. doi:10.1039/C8MD00472B
33. Chander S, Tang CR, Al-Maqtari HM, et al. Synthesis and study of anti-HIV-1 RT activity of 5-benzoyl-4-methyl-1,3,4,5-tetrahydro-2H-1,5-benzodiazepin-2-one derivatives. *Bioorg Chem*. 2017;72:74-79. doi:10.1016/j.bioorg.2017.03.013
34. Wee P, Wang Z. Epidermal growth factor receptor cell proliferation signaling pathways. *Cancers (Basel)*. 2017;9(5). doi:10.3390/cancers9050052
35. Van Nguyen C, Nguyen QT, Vu HTN, Phung HT, Pham KH, Le RD. Combined p53 and Bcl2 immunophenotypes in prognosis of vietnamese invasive breast carcinoma: A single institutional retrospective analysis. *Technol Cancer Res Treat*. 2020;19. doi:10.1177/1533033820983081
36. Shi P, Xu J, Cui H. The recent research progress of NF-κB signaling on the proliferation, migration, invasion, immune escape and drug resistance of glioblastoma. *Int J Mol Sci*. 2023;24(12). doi:10.3390/ijms241210337
37. Qodir N, Pramudhito D, Legiran, et al. Tumor necrosis factor-alpha and its association with breast cancer: A systematic review. *World J Oncol*. 2025;16(2):143-151. doi:10.14740/wjon2532
38. Gharge S, Gudasi S, Koli R. Targeting MDA-MB-231 cells using *Ailanthus excelsa* Roxb: A virtual binding evaluation, molecular flexibility analysis, and cytotoxicity study. *In Silico Research in Biomedicine*. 2025;1:100064. doi:10.1016/j.insi.2025.100064
39. Elsori D, Pandey P, Ramniwas S, et al. Naringenin as potent anticancer phytocompound in breast carcinoma: from mechanistic approach to nanoformulations based therapeutics. *Front Pharmacol*. 2024;15. doi:10.3389/fphar.2024.1406619
40. Hsu PH, Chen WH, Juanlu C, et al. Hesperidin and chlorogenic acid synergistically inhibit the growth of breast cancer cells via estrogen receptor/mitochondrial pathway. *Life*. 2021;11(9). doi:10.3390/life11090950
41. Bender O, Atalay A. Evaluation of anti-proliferative and cytotoxic effects of chlorogenic acid on breast cancer cell lines by real-time, label-free and high-throughput screening. *Marmara Pharm J*. 2018;22(2):173-179. doi:10.12991/mpj.2018.54
42. Ranganathan S, Halagowder D, Sivasithambaram ND. Quercetin suppresses twist to induce apoptosis in MCF-7 breast cancer cells. *PLoS One*. 2015;10(10). doi:10.1371/journal.pone.0141370
43. Wu ZY, Qiu KY, Gai YJ, Wu JH, Zhou BX, Shi QF. Quercetin: A natural ally in combating breast cancer. *Int J Nanomedicine*. 2025;20:9155-9177. doi:10.2147/IJN.S518174
44. Hashemzaei M, Far AD, Yari A, et al. Anticancer and apoptosis-inducing effects of quercetin in vitro and in vivo. *Oncol Rep*. 2017;38(2):819-828. doi:10.3892/or.2017.5766
45. Di Camillo Orfali G, Duarte AC, Bonadio V, et al. Review of anticancer mechanisms of isoquercitin. *World J Clin Oncol*. 2016;7(2):189-199. doi:10.5306/wjco.v7.i2.189

46. Gao XY, Li XY, Zhang CY, Bai CY. Scopoletin: a review of its pharmacology, pharmacokinetics, and toxicity. *Front Pharmacol*. 2024;15. doi:10.3389/fphar.2024.1268464

47. Singh SK, Srivastav AK, Chaurasiya S, Patel S, Kumar U, Kulhari H. Nanoencapsulation of morin hydrate with BSA for sustained drug release in colorectal carcinoma cells: experimental and computational approach. *Frontiers in Drug Delivery*. 2025;5. doi:10.3389/fddev.2025.1623317